J. Phys. A: Math. Theor. **46** (2013) 205203 (15pp) doi:10.1088/1751-8113/46/20/205203

Exact nonparaxial transmission of subwavelength detail using superoscillations

M V Berry

H H Wills Physics Laboratory, Tyndall Avenue, Bristol BS8 1TL, UK

E-mail: asymptotico@bristol.ac.uk

Received 5 February 2013, in final form 15 April 2013
Published 7 May 2013
Online at stacks.iop.org/JPhysA/46/205203

Abstract

Any object, described by a target function that need not be band-limited, can be sampled at any chosen set of points and then propagated without evanescent waves, using a function which is band-limited, so as to be imaged exactly (i.e. nonparaxially) at multiples of a given repetition distance. If the samples span a sub-wavelength region, the repeated images are superoscillatory. The number N of samples is equal to the repetition distance measured in wavelengths and also to the number of plane waves in the propagating field. If $N \gg 1$, the waves form a quasi-continuum, and asymptotics enables an almost-explicit description of the superoscillations. But the matrix involved is ill-conditioned (many of its eigenvalues are very small), so this method of sub-wavelength imaging would be pathologically sensitive to noise, and the depth of focus is exponentially small.

PACS numbers: 02.30.Mv, 02.30.Tb, 03.65.Ge, 42.25.Fx, 42.30.Kq, 42.30.Va

1. Introduction

There is considerable current interest in imaging objects with detail on scales smaller than the interrogating wavelength. Some techniques involve detecting the evanescent waves that commonly encode the sub-wavelength information [1, 2]. Perhaps the most promising alternative [3, 4] reconstructs the evanescent information by extrapolating the propagating fields in a way that exploits the sparse nature of the vectors which, in a suitable basis, represent many types of object.

My aim here is to explore a different possibility for superresolution, in which there are no evanescent waves, and the fine detail is present as low-amplitude superoscillatory structure in the fields that represent the objects. Superoscillations denote detail in band-limited functions on scales smaller than that corresponding to their largest Fourier component [5–13]. A difficulty with such schemes is that superoscillation is a delicate coherent almost-destructive interference phenomenon that is usually rapidly obscured by propagation. For the paraxial wave equation (or, equivalently, the time-dependent Schrödinger equation), superoscillations persist slightly further than evanescent waves [14], but (except in a limiting case [15]) do not survive into the far field or even the Fresnel region. Our concern here is not with the paraxial wave equation but

with the Helmholtz equation, where fine detail, including superoscillations, soon gets blurred on the wavelength scale, except for special schemes such as the one to be explored here. Some progress has been made by adapting pre-superoscillatory concepts from radar theory [16–21] to optics [22–24].

I will investigate a variant of the recent suggestion [25] to use nondiffracting beams, in which superoscillatory structure is exactly preserved under propagation. The variant is to devise superoscillatory fields that repeat exactly at multiples of a specified propagation distance (section 2). This gives increased flexibility for representing sub-wavelength structure, with the unfamiliar feature that the band-limited discrete spectrum representing the objects has an unusual form. The scheme can be expressed in convenient dimensionless form (section 3), and illustrated numerically (section 4).

The exact repetition studied here is the Montgomery effect [26]. It should be distinguished from the Talbot effect [27, 28] which it superficially resembles. The Talbot effect refers to laterally periodic objects, and is an asymptotically emergent phenomenon, with exact repetition under propagation only in the paraxial-optics limit. The relation between the Talbot and Montgomery effects is well understood [26, 29]. Nonparaxial effects blur the Talbot repetitions, with detail at propagation distance z obscured on a lateral scale which for wavelength λ is approximately $\Delta x = (z\lambda^3)^{1/4}$ [28, 30]. The Talbot repetition distance is d^2/λ, where d is the lateral repeat period of the object, so the blurring scale is $\Delta x = \sqrt{d\lambda}$—greatly exceeding λ under conditions $d \gg \lambda$ (necessary for near-paraxial propagation), and so obscuring any sub-wavelength structure. By contrast, for the exact repetitions in the scheme considered here the fields are not paraxial and the object fields need not be laterally periodic.

Underlying the procedure is a class of ill-conditioned (i.e. with many small eigenvalues) matrices, whose spectrum is studied in section 5. These matrices are related to those identified in the different context of an insightful study of optimization of superoscillatory functions [31]. When the field repeat distance is many wavelengths, the spectrum (of the optical field, not the associated matrices) can be approximated by a continuum, with an interesting mathematical structure discussed in section 6.

I am not proposing these repeating superoscillations as an immediately practical technique for superresolution microscopy. In addition to the extreme sensitivity of exponentially weak superoscillations to noise, the depth of focus, that is, the interval around each repetition distance in which the subwavelength detail is reproduced, is extraordinarily small (section 7). Rather, my aim is to draw attention to these z-periodic superoscillatory fields, and encourage further study of them.

2. Repeating propagation

We consider monochromatic scalar fields Ψ with wavenumber $k = 2\pi/\lambda$, propagating into the positive z direction from one-dimensional object fields and satisfying the Helmholtz equation in two space dimensions:

$$\nabla^2\Psi + k^2\Psi = 0, \quad k = \frac{2\pi}{\lambda}, \quad \Psi = \Psi(x, z). \tag{2.1}$$

Fields that repeat at multiples of the propagation distance H and contain no evanescent waves are represented by the finite superposition (Montgomery effect [26])

$$\Psi = \sum_{n=1}^{N} \exp\left\{ \mathrm{i}\left(\frac{2\pi z\,(n-1)}{H} \pm x\sqrt{k^2 - \left(\frac{2\pi\,(n-1)}{H}\right)^2} \right) \right\} c_{n,\pm}$$
$$N = \mathrm{int}\left(\frac{H}{\lambda}\right) + 1, \tag{2.2}$$

with arbitrary coefficients $c_{n,\pm}$. These are the fields to be studied here. From the viewpoint of creating superoscillations, the unusual feature is that the x dependence involves spatial frequencies that do not form an arithmetic progression but are given by the square root in (2.2). The number of plane waves equals the repetition distance, measured in wavelengths.

Such fields are not usually periodic in x. Periodicity with period L is a special case [32, 33]. It would require pairs of integers (m, n) satisfying

$$\sqrt{k^2-\left(\frac{2\pi\ (n-1)}{H}\right)^2}=\frac{2\pi m}{L},\quad \text{i.e. } m^2+(n-1)^2\left(\frac{L}{H}\right)^2=\left(\frac{L}{\lambda}\right)^2. \tag{2.3}$$

This is a diophantine equation that possesses solutions only if L and H are rational multiples of λ. Even then, the number of (m, n) pairs is small. In the most favourable case $L = H$, which requires

$$m^2+(n-1)^2=N^2, \tag{2.4}$$

the number of contributions to the sum (2.2) equals the number of ways the integer N can be written as the sum of two squares. This is much smaller than N: for $N \gg 1$, the fraction of integers that can be so written in more than one way is proportional to $1/\sqrt{\log N}$ [34, 35], and for such rare integers the number of ways is proportional to $\sqrt{\log N}$. Although it is possible to reproduce superoscillatory laterally periodic fields of this type, according to the procedure to be explained later, we do not consider this special case further.

If the sum (2.2) contains only a single n, it corresponds to a superposition of one or two waves (corresponding to $c_{n,+}$ and/or $c_{n,-}$), and the field propagates diffractionlessly, that is with intensity independent of z. This is the one-dimensional counterpart of the diffractionless scheme introduced earlier [25]. Two waves is too meagre a superposition to represent a superoscillatory object. Nevertheless, one-dimensional superoscillatory objects given by the fields (2.2) with $z = 0$ can be represented diffractionlessly, as sections $y = 0$ of two-dimensional objects in the (x, y) plane, the recipe, corresponding to waves with wavenumber k_0, is

$$\Psi=\exp\left(\mathrm{i}z\sqrt{k_0^2-k^2}\right)\sum_{n=1}^{N}\exp\left\{\mathrm{i}\left(\frac{2\pi y\ (n-1)}{H}\pm x\sqrt{k^2-\left(\frac{2\pi\ (n-1)}{H}\right)^2}\right)\right\}c_{n,\pm}. \tag{2.5}$$

This is a special case of the diffractionless scheme of [25]: a superposition with wavevectors lying on a cone with semiangle $\sin^{-1}k/k_0$. (The explicit recipe in [25] employs Bessel beams, but the authors recognize the possibility of a wider class of diffractionless beams, for example those involving plane waves as in (2.5).)

The analogous variant of the z-repeating (Montgomery) scheme (2.2) that generates two-dimensional fields is

$$\Psi=\sum_{n=1}^{N}\sum_{m=1}^{M}c_{n,m}\exp\left\{\mathrm{i}\left(\frac{2\pi z\ (n-1)}{H}+\sqrt{k^2-\left(\frac{2\pi\ (n-1)}{H}\right)^2}\ (x\cos\phi_m+y\sin\phi_m)\right)\right\}, \tag{2.6}$$

in which the ϕ_m are arbitrary angles. This is a superposition of plane waves with wavevectors on a series of coaxial cones with semiangles $\cos^{-1}((n-1)\lambda/H)$.

3. Dimensionless version

Returning to (2.2), it is convenient to introduce dimensionless variables. The natural z scale is the repeat distance H. For x, we introduce the distance D over which we seek to reproduce detail in an object; therefore we choose the new variables

$$\zeta\equiv\frac{2\pi}{H}z,\quad \xi\equiv\frac{x}{D},\quad q\equiv\frac{kH}{2\pi}=\frac{H}{\lambda},\quad A\equiv\frac{kD}{2\pi}=\frac{D}{\lambda}. \tag{3.1}$$

For superresolution, $D < \lambda$, so we are interested in $A < 1$. Extreme superoscillation corresponds to the small-A limit; this is a delicate matter and will be discussed in section 6. After scaling, (2.2) becomes

$$\Psi(x,z) = \psi(\xi,\zeta) = \sum_{n=1}^{N(q)} \exp\left\{ \mathrm{i}\left(\zeta(n-1) \pm 2\pi A\xi\sqrt{1-(n-1)^2/q^2} \right) \right\} c_{n,\pm}$$
$$N(q) = \mathrm{int}(q) + 1. \tag{3.2}$$

For $z = 0$, this gives the class of objects that self-reproduce repeatedly:

$$\psi(\xi,0) \equiv f(\xi) = \sum_{n=1}^{N(q)} \exp\left(\mathrm{i}2\pi A\xi\sqrt{1-(n-1)^2/q^2}\right) c_{n,\pm}. \tag{3.3}$$

These functions $f(\xi)$ are band-limited; they contain only spatial frequencies $\leqslant A$, so they are superoscillatory if they contain detail on ξ scales smaller than $1/A$—sub-wavelength because $\xi < 1/A$ corresponds to $x < \lambda$. We wish to employ such functions to represent objects with sub-wavelength structure, described by a 'target function' $F(\xi)$ that is usually not band-limited.

There are several ways to create this representation—that is, to represent the non-band-limited target $F(\xi)$ by the band-limited $f(\xi)$. Some are Fourier-based [5, 19], but we follow a different route [9, 10, 25, 31], by requiring $f(\xi)$ to coincide with $F(\xi)$ at a series of N sample points ξ_m, chosen to include the region of the sub-wavelength structure of interest. It will suffice to consider objects symmetrical about $\xi = 0$, so $f(\xi)$ and $F(\xi)$ are even functions. Thus, in the initial plane $\zeta = 0$,

$$f(\xi) = \sum_{n=1}^{N(q)} \cos\left(2\pi A\xi\sqrt{1-\left(\frac{n-1}{q}\right)^2} \right) c_n, \tag{3.4}$$

and

$$F(\xi_m) = f(\xi_m) \equiv f_m = \sum_{n=1}^{N(q)} \cos\left(2\pi A\xi_m\sqrt{1-\left(\frac{n-1}{q}\right)^2} \right) c_n \equiv \sum_{n=1}^{N(q)} M_{mn}\, c_n,$$
$$(1 \leqslant m \leqslant N(q), \quad 0 \leqslant \xi_m \leqslant 1) \tag{3.5}$$

in which the restriction $\xi_m < 1$ corresponds to the decision to represent objects with $|x| < D$. We are interested in $A < 1$, so $|\xi| < 1$ corresponds to the sub-wavelength detail of interest here, with the degree of superresolution quantified by $A^{-1} = \lambda/D$.

The coefficients are determined by inverting the $N \times N$ matrix M in (3.5) and letting this act on the target vector with coefficients f_m:

$$c_n = \sum_{m=1}^{N(q)} (M^{-1})_{nm}\, f_m. \tag{3.6}$$

To implement the scheme, it is necessary to choose the N sampling points ξ_m. The most natural way might seem to be points uniformly distributed on $0 \leqslant \xi_m \leqslant 1$. However, a convenient alternative is to make the unique choice of ξ_m which makes M a real symmetric matrix. Thus

$$\xi_m = \sqrt{1-(m-1)^2/q^2},$$
$$M_{mn} = \cos\left(2\pi A\sqrt{(1-(m-1)^2/q^2)(1-(n-1)^2/q^2)}\right). \tag{3.7}$$

Numerical comparisons (not given here) indicate that the details of the distribution of ξ_m do not greatly influence the effectiveness of the reconstruction. But one advantage of the choice

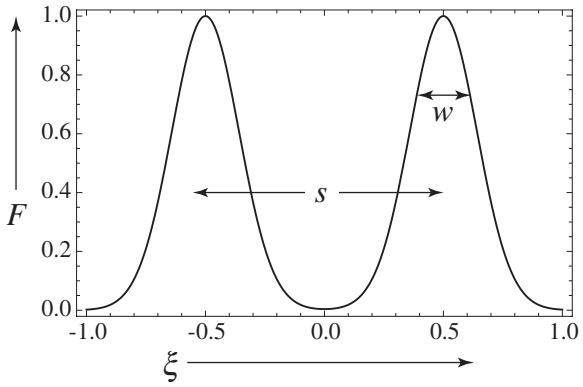

Figure 1. Target image wave $F(\xi)$ (equation (4.1)) for $s = 1$, $w = 1/5$.

in (3.7) over the uniform distribution is that its concentration of points near $\xi = 1$ gives a better representation near this extreme of the sampling region, which as we will see is where the superoscillations give way to a dramatic increase in $f(\xi)$ for $\xi > 1$.

The effectiveness of the reconstruction depends on the spectrum of M, that is on its (real) eigenvalues λ_l and orthonormal eigenvectors $u_{j,n}$ determined by

$$\sum_{n=1}^{N(q)} M_{mn}\, u_{j,\,n} = \lambda_j u_{j,\,m}. \tag{3.8}$$

As we will see in sections 5 and 6, many of the eigenvalues are very small, so M is ill-conditioned, with disappointing consequences. The coefficients f_m in the target vector can be projected onto the eigenbasis; thus

$$f_m = \sum_{j=1}^{N(q)} d_j\, u_{j,\,m}, \quad d_j = \sum_{m=1}^{N(q)} u_{j,\,m} f_m. \tag{3.9}$$

In this representation, the coefficients in the function $f(\xi)$ in (3.4) are

$$c_n = \sum_{j=1}^{N(q)} \lambda_j^{-1} \left(\sum_{m=1}^{N(q)} u_{j,\,m} f_m \right) u_{j,\,n}. \tag{3.10}$$

4. Numerical illustration

For the target function in numerical calculations, we take two Gaussians separated by a ξ distance s, corresponding to an x distance $sD = sA\lambda$, each with ξ width w, i.e. x width $wD = wA\lambda$ (figure 1):

$$F\,(\xi) = \exp\left(-\frac{\left(\xi - \frac{1}{2}s\right)^2}{w^2} \right) + \exp\left(-\frac{\left(\xi + \frac{1}{2}s\right)^2}{w^2} \right). \tag{4.1}$$

Figure 2(*a*) shows how accurately the rendered object function $f(\xi)$, calculated from (3.4) with coefficients (3.6), reproduces the target $F(\xi)$ in the sampled interval, including sub-wavelength detail on the scale $\lambda/20$ of the width of the peaks. To achieve this degree of superoscillation, it was necessary to perform the computations with high precision: with anything less than 50-digit accuracy, the rendering failed because of the ill-conditioned

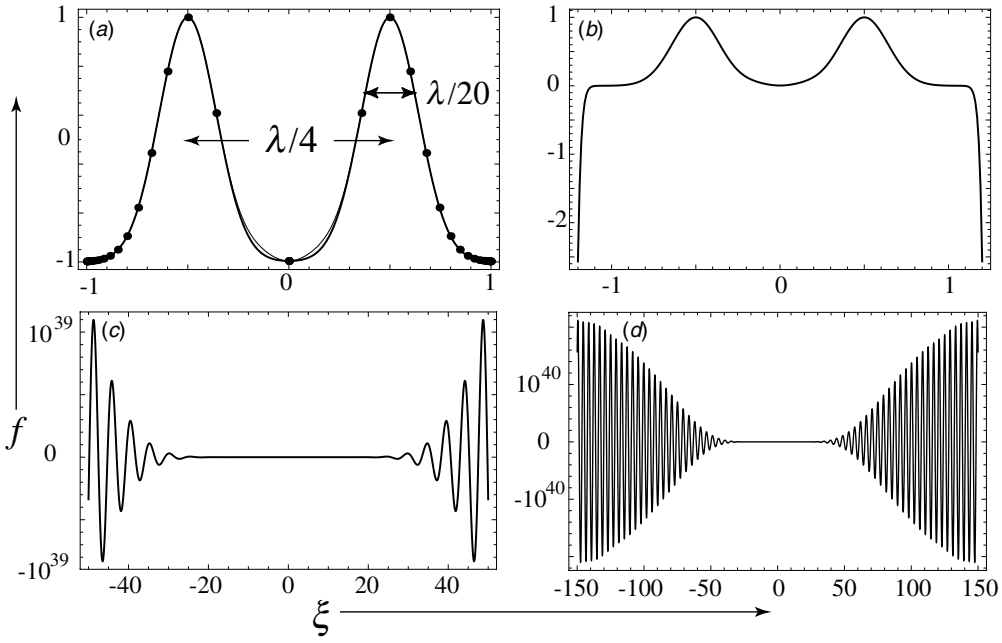

Figure 2. Superoscillatory rendering $f(\xi)$ (3.4) of target wave $F(\xi)$ (4.1) with parameters in figure 1, for $A = 1/4$, i.e. Gaussian peaks with width $\lambda/20$ separated by $\lambda/4$, and $q = 15$ (i.e. 31 sampled points in $|\xi| \leqslant 1$), and a z periodicity of 15λ. (*a*) rendered over the sampled interval $|\xi| \leqslant 1$ (thick curve), showing the sampled points (dots) and the target image (thin curve). (*b*) Rendered over the interval $|\xi| \leqslant 1.2$, showing the rapid deviation from the target outside the sampled interval. (*c*) Rendered over the interval $|\xi| \leqslant 50$, and (*d*) over the interval $|\xi| \leqslant 150$, showing the development of oscillations with period λ, corresponding to a ξ range $1/A = 4$.

nature of the matrix M. The physical counterpart of this numerical sensitivity would be a pathological sensitivity of this degree of superresolution to noise. This is confirmed by numerical simulations (not shown here) in which weak random noise is added to the coefficients c_n in (3.4). The sensitivity arises because the c_n are very large (of order 10^{46} in the simulation of figure 2) and alternate in sign, again reflecting the fact that superoscillation arises from almost-complete destructive interference.

Concomitantly, and as figures 2(*b*)–(*d*) illustrate, the superoscillatory simulacrum $f(\xi)$ deviates dramatically from the target $F(x)$ outside the sampled interval $|\xi| < 1$. This phenomenon, that functions are exponentially smaller where they superoscillate than where they oscillate as their Fourier content would suggest, is the familiar penalty associated with superoscillations [5, 31]. It would be interesting to explore whether recently-developed techniques [31] for optimizing superoscillations can be applied to functions of the type (3.4); this would amount to minimizing the vast excursions for $|\xi| > 1$.

5. Spectrum

The matrix M in (3.7) is Hermitian, so its eigenvalues λ_j are real. Numerical exploration suggests that when ordered according to their magnitude ($|\lambda_1| > |\lambda_2| > \ldots$) the λ_j alternate in sign, except for some cases with $A \gg 1$ and small q (fortunately, regimes not of interest for superoscillation); an explanation of this for small A will be presented in section 6, but

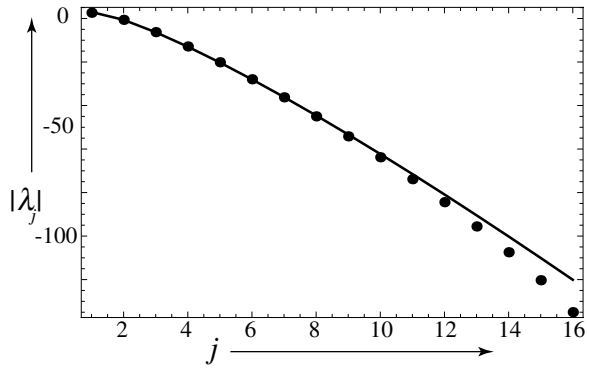

Figure 3. Moduli $|\lambda_j|$ of eigenvalues of the matrix M in (3.7), for $A = 1/8$ and $q = 15$ (dots), compared with theoretical small A formula (6.9) for $q|\Lambda_j|$ (cf (6.1)) (curve). These eigenvalues alternate in sign.

a fuller analytical understanding would be desirable. Figure 3 illustrates a typical case; the logarithmic plot indicates a long tail of exponentially small eigenvalues, reflecting the fact that M is ill-conditioned.

Figure 4 illustrates a typical set of eigenvectors $u_{j,n}$, ordered according to eigenvalue magnitude as in figure 3, with each eigenvector, labelled j, plotted as a function of its component index n. The earlier eigenvectors—indeed all except the highest few, i.e. $j \sim N$—resemble samplings of smooth functions, and extensive computation indicates that this behaviour is almost insensitive to the value of A unless $A \gg 1$. These observations will be explained in the next section.

6. Short-wave and continuum limits

When $q \gg 1$, that is when the z repeat distance greatly exceeds the wavelength (cf (3.1)), the wavevectors labelled n in (3.2–3.5) are numerous and close together, motivating a continuum approximation. Natural variables are

$$X \equiv \frac{m-1}{q}, \quad Y \equiv \frac{n-1}{q}, \quad \Lambda_j \equiv \frac{\lambda_j}{q}, \quad u_j(X) \equiv u_{j,m}\sqrt{q}. \tag{6.1}$$

Thus the eigenequation (3.8) becomes

$$\int_0^1 \mathrm{d}Y M(X,Y;A)u_j(Y) = \Lambda_j u_j(X), \tag{6.2}$$

in which M is now an integral operator—we denote it $M(A)$—with kernel

$$M(X,Y;A) \equiv \cos\left(2\pi A\sqrt{1-X^2}\sqrt{1-Y^2}\right). \tag{6.3}$$

Since $M(A)$ acts on even functions with $0 \leqslant X, Y \leqslant 1$, a natural orthonormal basis is the even-order Legendre polynomials, namely [36]

$$u_j^{(0)}(X) = \sqrt{4j-3}P_{2(j-1)}(X), \quad j = 1, 2, 3 \ldots . \tag{6.4}$$

We are especially interested in the small-A regime, because as we have seen this corresponds to superoscillatory functions. In the limit $A = 0$, the Legendre basis is exact:

$$\int_0^1 \mathrm{d}Y M(X,Y;0)u_j^{(0)}(Y) = \int_0^1 \mathrm{d}Y u_j^{(0)}(Y) = \delta_{j,1}u_j^{(0)}(X), \tag{6.5}$$

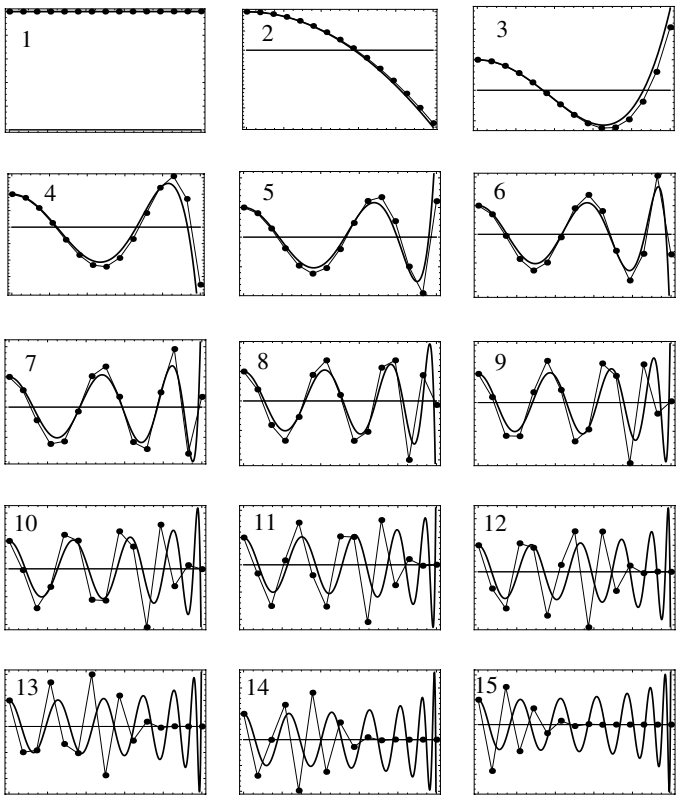

Figure 4. Eigenvectors $u_{j,m}$ of the discrete matrix M_{mn} in (3.7) (dots joined by thin lines), and eigenfunctions $u_j(X)$ (equation (6.4)) of the continuum approximation matrix $M(X,Y;A)$ (equation (6.3)) (thick curves), for the indicated values of j, calculated for $q = 14$ and (for the discrete matrix) for $A = 1/80$. The horizontal axes correspond to $0 \leqslant (m-1)/q \leqslant 1$ and $0 \leqslant X \leqslant 1$ for the two sets of eigenfunctions, both of which are normalized to unity at the origin.

so the zero-order eigenvalues are

$$\Lambda_j\,(A=0) = \delta_{j,1}. \tag{6.6}$$

The infinitely many zero eigenvalues mean that $M(0)$ is non-invertible (i.e. infinitely ill-conditioned), so we need to do a little better, and seek the lowest-order small-A approximation for which the eigenvalues are non-zero.

In the Legendre basis, the coefficients of powers of A conveniently factorize in the matrix elements of $M(A)$:

$$\begin{aligned}\langle i\,|M(A)\,|j\rangle &= \int_0^1 \mathrm{d}X \int_0^1 \mathrm{d}Y\, u_i^{(0)}(X)\cos\left(2\pi A\sqrt{1-X^2}\sqrt{1-Y^2}\right)u_i^{(0)}(Y)\\ &= \sum_{s=1}^{\infty}(-1)^{s-1}\frac{(2\pi A)^{2s-2}}{(2s-2)!}h_{si}h_{sj},\end{aligned} \tag{6.7}$$

involving the numbers

$$\begin{aligned}h_{si} &= \int_0^1 \mathrm{d}X\,(1-X^2)^{s-1}u_i^{(0)}(X)\\ &= \Gamma\,(s)\,\sqrt{4i-3}\sum_{t=i-1}^{s-1}(-1)^t\frac{\Gamma\left(t+\frac{1}{2}\right)}{2\Gamma\,(s-t)\,\Gamma\,(2-i+t)\,\Gamma\left(i+t+\frac{1}{2}\right)},\end{aligned} \tag{6.8}$$

Table 1. The numbers h_{si} for small s, i.

$s\backslash i$	$i=1$	$i=2$	$i=3$	$i=4$	$i=5$
$s=1$	1	0	0	0	0
$s=2$	$\frac{2}{3}$	$-\frac{2}{3\sqrt{5}}$	0	0	0
$s=3$	$\frac{8}{15}$	$-\frac{16}{21\sqrt{5}}$	$\frac{8}{105}$	0	0
$s=4$	$\frac{16}{35}$	$-\frac{16}{21\sqrt{5}}$	$\frac{48}{385}$	$-\frac{16}{231\sqrt{13}}$	0
$s=5$	$\frac{128}{315}$	$-\frac{512}{693\sqrt{5}}$	$\frac{768}{5005}$	$\frac{-512}{3465\sqrt{13}}$	$\frac{128}{6435\sqrt{17}}$

Table 2. Small-A eigenvalue coefficients.

j	1	2	3	4	5
$\Lambda_j/\,(2\pi A)^{2j-2}$	1	$-\frac{2}{45}$	$\frac{8}{33\ 075}$	$-\frac{16}{31\ 216\ 185}$	$\frac{128}{221\ 746\ 399\ 875}$

with the important property that $h_{si}=0$ if $i>s$. The diagonal coefficients can be evaluated in closed form:

$$h_{ss}=(-1)^{s-1}\,\frac{4^{s-1}\,[(2s-2)!]^2}{(4s-4)!\sqrt{4s-3}}. \tag{6.9}$$

Table 1 shows the first few coefficients.

Thus the desired lowest-order eigenvalues are the small-A diagonal elements:

$$\begin{aligned}\frac{\Lambda_j\,(A)}{(2\pi A)^{2j-2}}&=(-1)^{j-1}\,\frac{\left(h_{jj}\right)^2}{(2j-2)!}+O\left(A^2\right)\\&=\frac{(-16)^{j-1}\,[(2j-2)!]^3}{(4j-4)!\,(4j-3)!}+O\left(A^2\right)\quad j=1,2,3\ldots.\end{aligned} \tag{6.10}$$

Table 2 shows the first few coefficients. And as figure 3 and other computations (not shown) indicate, the lowest-order approximation accurately represents all but the smallest few eigenvalues (i.e. $j\sim N$). For the eigenvectors, the Legendre basis (6.4) is the lowest-order small A approximation, and figure 4 shows that as with the eigenvalues it accurately represents the exact vectors except for the few with $j\sim N$. Standard perturbation theory applied to the operator (6.7) gives the first corrections as

$$\begin{aligned}u_j(X)&=u_j^{(0)}(X)+(2\pi A)^2\left(-e_{j-1}u_{j-1}^{(0)}(X)+e_ju_{j-1}^{(0)}(X)\right)+O\left(A^4\right)\\e_1&=\tfrac{2}{9\sqrt{5}},\quad e_2=\tfrac{8}{147\sqrt{5}},\quad e_3=\tfrac{6}{121\sqrt{13}},\quad\ldots.\end{aligned} \tag{6.11}$$

With this understanding of the spectrum, we can now seek the large q, small A approximation to the superoscillatory representation $f(\xi)$ of the target $F(\xi)$. The continuum approximation for the representation (3.9), giving $f(\xi)$ as a series including $N_{\max}$ eigenvectors, is

$$f_{\mathrm{cont},N_{\max}}\,(\xi)=\sum_{j=1}^{N_{\max}}d_ju_j^{(0)}\left(\sqrt{1-\xi^2}\right), \tag{6.12}$$

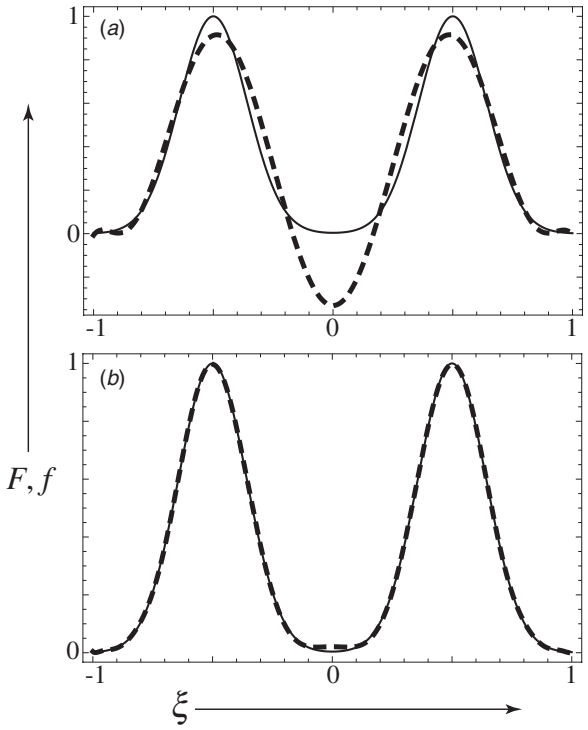

Figure 5. Full curves: target image wave $F(\xi)$ as in figure 1; dashed curves: continuum approximation for superoscillatory reconstruction $f(\xi)$ (equations (6.12—6.13)), including n coefficients F_j, where (a) $n = 5$, (b) $n = 10$.

with the coefficients

$$d_j = \int_0^1 \mathrm{d}X\, F\left(\sqrt{1-X^2}\right) u_j^{(0)}(X). \tag{6.13}$$

Numerical evidence, supported by some rudimentary asymptotics, indicates that the sequence of $|d_j|$ converges exponentially. As a consequence, the sum over j converges if $|\xi| < 1$, so the limit $N_{\max} \to \infty$ makes sense—that is, (6.12) reproduces the target $F(\xi)$ accurately in the sampled range. This is illustrated in figure 5.

But for large $|\xi|$ the series does not converge, because the convergence of the sequence of $|d_j|$ is always foiled by the exponential divergence of the Legendre eigenvectors in (6.12), which for large ξ, i.e. large imaginary argument X, diverge as $|X|^{2j-2}$. This divergence is not a defect of the continuum asymptotics, because the superoscillatory rendering $f(\xi)$, given exactly by the discrete sum over $N(q)$ plane waves in section 3, also fails to converge outside the target region as the number of plane waves increases, that is, as the specified z repeat distance increases and, consequently, the target object is sampled more finely. In fact the continuum approximation is rather accurate if the limit $N_{\max}$ of the sum in (6.12) is chosen as $N(q)$. This is illustrated in figure 6 (readers wishing to repeat these computations should note that several-hundred digit precision was required to achieve numerical stability). By contrast (and as indicated by further computations—not shown), the limit $A \to 0$ with $q \gg 1$ fixed does converge, and is accurately given by the continuum approximation.

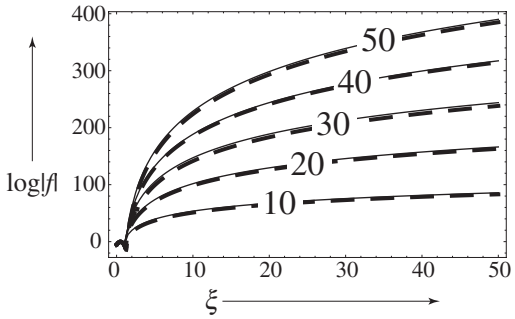

Figure 6. Full curves: continuum approximation (6.12) for the superoscillatory representation $f(\xi)$ of the target $F(\xi)$ of figure 1, outside the target region $|\xi| \leqslant 1$, with $N_{\max} = N(q)$, for the indicated values of q; dashed curves: $f(\xi)$ calculated from the discrete plane-wave sum (3.4) for $A = 1/80$.

7. Depth of focus

In the ξ, ζ plane, the even-ξ waves that we have been considering are, from (3.3) and (3.4),

$$\psi(\xi, \zeta) = \sum_{n=1}^{N(q)} \exp(\mathrm{i}\zeta(n-1)) \cos\left(2\pi A\xi\sqrt{1-(n-1)^2/q^2}\right)c_n, \tag{7.1}$$

with c_n given by (3.10). Since these coefficients alternate in sign, in ways strongly correlated with the trignometric factor involving ξ (in the target interval $|\xi| \leqslant 1$), we can expect the delicate interference responsible for the superoscillations to be rapidly destroyed by the phase factor involving ζ when ζ deviates from one of the repetition distances, which in these scaled variables are multiples of 2π. Alternatively stated, the depth of focus, defined as the distance surrounding each repetition within which the superoscillations survive, will be very small. It will suffice to consider the neighbourhood of $\zeta = 0$. We expect $|\psi|$ to rise to very large values away from $\zeta = 0$, similarly to the large values we have seen for $|\xi| > 1$ when $\zeta = 0$.

Figure 7 illustrates the pathological sensitivity of $|\psi|$ and its superoscillations to deviations from $\zeta = 0$, and figure 8 shows the rise from of order unity to enormous values halfway between repetitions, i.e. $\zeta = \pi$. Explicitly, for the example in figure 7, where the z repeat distance is 15λ and the sampled interval $(-1 \leqslant \xi \leqslant 1)$ is $\lambda/4$, superoscillations are confined to an interval $\Delta\zeta < 10^{-45}$, so the depth of focus is (cf (3.1)) $\Delta z = \Delta\zeta\,(q/2\pi)\lambda \sim 10^{-45}\lambda$.

This needs to be explained. To get an order of magnitude estimate for Δz, it will suffice to consider the symmetry line $\xi = 0$, on which the field (7.1) is

$$\psi(0, \zeta) = \sum_{n=1}^{N(q)} \exp(\mathrm{i}\zeta(n-1))\, c_n. \tag{7.2}$$

As we will soon see, the coefficients c_n are very large, and as already mentioned they alternate in sign for the small A of interest here, giving rise to an almost-cancellation at $\zeta = 0$, where ψ is of order unity. By contrast, halfway between repetitions, that is at $\zeta = \pi$, the contributions add constructively, and ψ rises to its maximum value (cf figure 8):

$$\psi_{\max} \equiv |\psi(0, \pi)| = \left|\sum_{n=1}^{N(q)} (-1)^{n-1} c_n\right| = \sum_{n=1}^{N(q)} |c_n|. \tag{7.3}$$

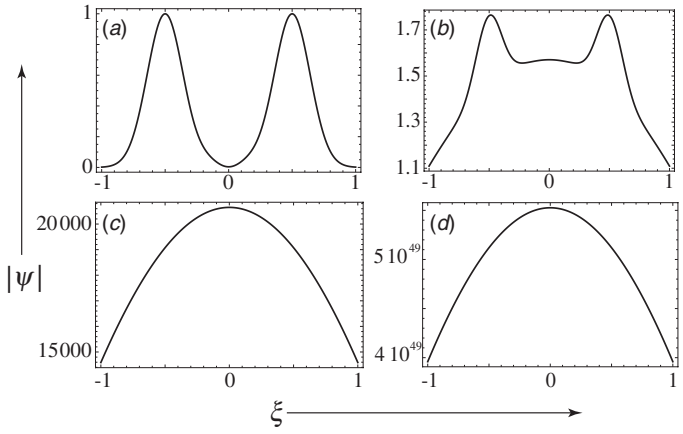

Figure 7. Destruction of superoscillations by propagation, illustrated by the modulus $|\psi(0,\zeta)|$, calculated from (7.1) with $A = 1/8$, $q = 15$, for (*a*) $\zeta = 0$, (*b*) $\zeta = 10^{-45}$, (*c*) $\zeta = 5 \times 10^{-45}$, (*d*) $\zeta = \pi$.

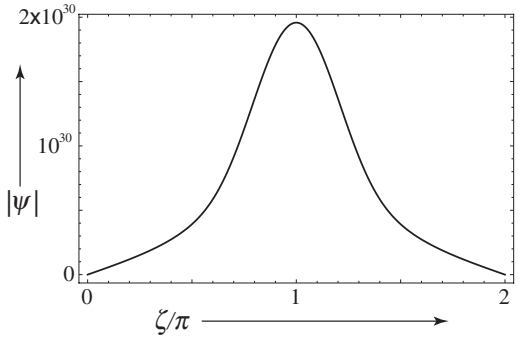

Figure 8. Modulus $|\psi(0,\zeta)|$ on the symmetry line $\xi = 0$, for one repetition period, calculated from (7.1) for $A = 1/8$, $q = 10$.

Similar in magnitude is the ζ-average value

$$\psi_{\rm av} \equiv \sqrt{\frac{1}{2\pi}\int_0^{2\pi} {\rm d}\zeta\, |\psi(0,\zeta)|^2} = \sqrt{\sum_{n=1}^{N(q)} c_n^2}. \tag{7.4}$$

Also similar is the magnitude of the initial slope

$$\psi' \equiv \left|\partial_\xi \psi(0,0)\right| = \left|\sum_{n=1}^{N(q)} (n-1)\, c_n\right|. \tag{7.5}$$

Numerics, and the estimate to follow, indicate that the c_n are similar in magnitude, so $|c_n|$ can be replaced by its average c. Then the three quantities just defined are, approximately,

$$\psi_{\rm max} \sim \sqrt{q}\psi_{\rm av} \sim \tfrac{1}{2}\psi' \sim qc. \tag{7.6}$$

To estimate qc, we use the continuum approximation of the previous section, from which (3.10) can be replaced by the function $C(Y;q)$, defined by

$$qc_n \approx C\,(Y;\,q) \equiv \sum_{j=1}^{N(q)} \Lambda_j^{-1} u_j^{(0)}\,(Y) \int_0^1 \mathrm{d}X\, u_j^{(0)}(X) f\left(\sqrt{1-X^2}\right)$$
$$= \sum_{j=1}^{N(q)} \Lambda_j^{-1} u_j^{(0)}\,(Y)\; d_j, \tag{7.7}$$

with d_j given by (6.13). For the average value c, we can replace the normalized eigenvectors $u_j^{(0)}\,(Y)$by their average value unity, so, using the approximation (6.10),

$$qc \sim C \equiv \sum_{j=1}^{N(q)} \left|\Lambda_j\right|^{-1} d_j \approx \sum_{j=1}^{N(q)} \frac{\alpha_j}{(2\pi A)^{2j-2}} \tag{7.8}$$

where

$$\alpha_j = \frac{(2j-2)!}{(h_{jj})^2}\, d_j, \tag{7.9}$$

with the numbers h_{jj} defined by (6.9). In the absence of a precise asymptotic estimate for the α_j, we rely on numerics, which indicate

$$\alpha_j \sim j^{\mu j}, \tag{7.10}$$

with $\mu \sim 2.5$ weakly dependent on the parameters s and w in the target object (4.1). Thus the terms in the sum (7.8) increase faster than exponentially with j, so the sum can be approximated by its largest term, giving

$$\psi_{\max} \sim C \sim \frac{(q+1)^{2.5(q+1)}}{(2\pi A)^{2q}}. \tag{7.11}$$

This rough asymptotics agrees with exact numerical computations of $\psi_{\max}$; for the case shown in figure 8, where $\psi_{\max} = 2 \times 10^{30}$, (7.11) gives $\psi_{\max} \sim 5 \times 10^{30}$.

The depth of focus Δz is approximately the distance over which $|\psi|$ rises beyond unity, so the foregoing considerations give

$$\frac{\Delta z}{\lambda} \sim \frac{1}{\psi'} \sim \frac{1}{C} \sim \frac{(2\pi A)^{2q}}{(q+1)^{2.5(q+1)}} = \left(\frac{D}{\lambda}\right)^{2H/\lambda} \left(\frac{H}{\lambda}+1\right)^{-2.5(H/\lambda+1)}. \tag{7.12}$$

This estimate explains the extreme sensitivity of the superoscillations to deviation from the repetition distance.

8. Concluding remarks

This study, based on the concept of superoscillations, has shown that it is possible in principle to propagate sub-wavelength information exactly, from an object plane to a sequence of equally spaced distant planes. The distinctive feature is the square root spectrum of transverse plane-wave components in the representation (2.2) and its dimensionless counterpart (3.2). 'Exactly' means reproducing the object at a number of sample points equal to the number of contributing plane waves in superpositions that are solutions of the Helmholtz equation which do not involve evanescent waves or the paraxial approximation. Restricting the propagation to a sequence of distances, rather than requiring diffractionless propagation for all distances as in the paper [25] (which partly inspired this complementary work), gives greater flexibility in the sampling of the object.

'In principle' means that, in common with all superoscillatory schemes to date, the propagation of sub-wavelength information carries a heavy price. The delicate coherent almost-destructive interference responsible for the reconstruction is pathologically vulnerable to noise, the reconstructed fields rise to enormous values outside the sampled region, and the depth of focus is tiny. Therefore this scheme is unlikely to be practicable, at least in its present form.

But the existence of a method [3] for propagating sub-wavelength information robustly, that is, in a way not pathologically sensitive to noise, raises an intriguing possibility. In that method, as in the scheme described here, there is a target object which is not band-limited (here it is $F(\xi)$, e.g. (4.1)), and its distant reconstruction depends only on band-limited variants constructed from this. Therefore it might be that the two ideas are related—that the robust method [3] can be re-expressed in terms of superoscillatory functions. Central to the robust method is the restriction to objects that are sparse in some basis, and the example (4.1) used here to illustrate the superoscillatory scheme involves only two parameters and so is also sparse in a basis of Gaussians. This possible connection deserves further exploration.

On the mathematical side, the effectiveness of reconstruction of two-dimensional objects should be studied. In addition, the large q asymptotics, corresponding to repetition distances of many wavelengths, or, equivalently, many sample points, should be developed beyond the continuum approximation discussed in section 6. In particular, the spectrum of the $N(q) \times N(q)$ matrix (3.7) needs to be understood in more detail, especially for the smallest eigenvalues and associated eigenvectors.

Acknowledgments

I thank Mark Dennis and Mordechai Segev for helpful discussions. My research is supported by the Leverhulme Trust. I also thank the Isaac Newton Institute for generous hospitality in the initial phases of this work.

References

[1] Hemmer P R and Zapata T 2012 The universal scaling laws that determine the achievable resolution in different schemes for superresolution imaging *J. Opt.* **14** 083002
[2] Lindberg J 2012 Mathematical concepts of optical superresolution *J. Opt.* **14** 083001
[3] Gazit S, Szameit A, Eldar Y and Segev M 2009 Super-resolution and reconstruction of sparse sub-wavelength images *Opt. Express* **17** 23920–46
Gazit S, Szameit A, Eldar Y and Segev M 2009 Super-resolution and reconstruction of sparse sub-wavelength images *Opt. Express* **18** 26631 (erratum)
[4] Shechtman Y, Gazit S, Szameit A, Eldar Y and Segev M 2010 Super-resolution and reconstruction of sparse images carried by incoherent light *Opt. Lett.* **35** 1148–50
[5] Berry M V 1994 Faster than Fourier *Quantum Coherence and Reality: In Celebration of the 60th Birthday of Yakir Aharonov* ed J S Anandan and J L Safko (Singapore: World Scientific) pp 55–65
[6] Ferreira P J S G and Kempf A 2006 Superoscillations: faster than the Nyquist rate *IEEE Trans. Signal Process.* **54** 3732–40
[7] Kempf A and Ferreira P J S G 2004 Unusual properties of superoscillating particles *J. Phys. A: Math. Gen.* **37** 12067–76
[8] Calder M S and Kempf A 2005 Analysis of superoscillatory wave functions *J. Math. Phys.* **46** 012101
[9] Bucklew J A and Saleh B E A 1985 Theorem for high-resolution high-contrast image synthesis *J. Opt. Soc. Am.* A **2** 1233–6
[10] Nashold K M, Buckew J A, Rudin W and Saleh B E A 1989 Synthesis of binary images from band-limited functions *J. Opt. Soc. Am.* A **6** 852–8
[11] Aharonov Y, Albert D Z and Vaidman L 1988 How the result of a measurement of a component of the spin of a spin-1/2 particle can turn out to be 100 *Phys. Rev. Lett.* **60** 1351–4
[12] Aharonov Y and Rohrlich D 2005 *Quantum Paradoxes: Quantum Theory for the Perplexed* (Weinheim: Wiley)

[13] Aharonov Y, Colombo F, Sabadini I, Struppa D C and Tollaksen J 2011 Some mathematical properties of superoscillations *J. Phys. A: Math. Theor.* **44** 365304
[14] Berry M V and Popescu S 2006 Evolution of quantum superoscillations, and optical superresolution without evanescent waves *J. Phys. A: Math. Gen.* **39** 6965–77
[15] Aharonov Y, Colombo F, Sabadini I, Struppa D C and Tollaksen J 2013 On the Cauchy problem for the Schrödinger equation with superoscillatory initial data *J. Math. Pures Appl.* **99** 165–73
[16] Schelkunoff S A 1943 A mathematical theory of linear arrays *Bell Syst. Tech. J.* **22** 80–107
[17] Wong A M H and Eleftheriades G V 2010 Superoscillatory radar imaging: improving radar range resolution beyond fundamental bandwidth limitations *IEEE Microw. Wirel. Compon. Lett.* **22** 147–9
[18] Wong A M H and Eleftheriades G V 2010 Adaptation of Schelkunoff's superdirective antenna theory for the realization of superoscillatory antenna arrays *IEEE Antennas Wirel. Propag. Lett.* **9** 315–218
[19] Berry M V 2013 Superoscillations, endfire and supergain *Aharonov 80th Birthday Festschrift: Fundamental Aspects of Quantum Theory: A Two-Time Winner* ed D C Struppa and J Tollaksen (Berlin: Springer) at press
[20] Cox H, Zeskind R M and Kooij T 1986 Practical supergain *IEEE Trans. Acoust. Speech Signal Process.* **34** 393–8
[21] Haviland R P 1995 Supergain antennas: possibilities and problems *IEEE Antennas Propag. Mag.* **37** 13–26
[22] Toraldo di Francia G 1952 Supergain antennas and optical resolving power *Suppl. Nuovo Cimento* **9** 426–38
[23] Leiserson I, Lipson S G and Sarafis V 2000 Superresolution in far-field imaging *Opt. Lett.* **25** 209–211
[24] Rogers E T F, Lindberg J, Roy T, Savo S, Chad J E, Dennis M R and Zheludev N I 2012 A super-oscillatory lens optical microscope for subwavelength imaging *Nature Mater.* **11** 432–5
[25] Makris K G and Psaltis D 2011 Superoscillatory diffraction-free beams *Opt. Lett.* **36** 4335–7
[26] Montgomery W D 1967 Self-imaging objects of infinite aperture *J. Opt. Soc. Am.* A **57** 772–8
[27] Patorski K 1989 The self-imaging phenomenon and its applications *Prog. Opt.* **27** 1–108
[28] Berry M V and Klein S 1996 Integer, fractional and fractal Talbot effects *J. Mod. Opt.* **43** 2139–64
[29] Lohmann A W, Knuppertz H and Jahns J 2005 Fractional Montgomery effect: a self-imaging phenomenon *J. Opt. Soc. Am.* A **22** 1500–8
[30] Ring J D, Lindberg J, Howls C J and Dennis M R 2012 Aberration-like cusped focusing in the post-paraxial Talbot effect *J. Opt.* **14** 075702
[31] Katsav E and Schwartz M 2013 Yield-optimised superoscillations *IEEE Trans. Signal Process.* at press (arXiv:1209.6572)
[32] Saastamoinen T, Tervo J, Vahimaa P and Turunen J 2004 Exact self-imaging of transversely periodic fields *J. Opt. Soc. Am.* A **21** 1424–9
[33] Jahns J and Lohmann A W 2009 Optical wave fields with lateral and longitudinal periodicity *Appl. Opt.* **48** 3438–45
[34] Landau E 1908 Über die Einteilung der positiven ganzen Zahlen in view Klassen nach der Mindezahl der zu ihrer additiven Zusammensetzung erfordlicher Quadrate *Arch. Math. Phys.* **13** 305–12
[35] Hardy G H 1999 *Ramanujan: Twelve Lectures on Subjects Suggested by his Life and Work* (New York: Chelsea)
[36] DLMF 2010 *NIST Handbook of Mathematical Functions* (Cambridge: Cambridge University Press) http://dlmf.nist.gov